Developmental Biology 473 (2021) 80–89

Contents lists available at ScienceDirect

Developmental Biology

journal homepage: www.elsevier.com/locate/developmentalbiology

VEGF signaling activates the matrix metalloproteinases, *MmpL7 and MmpL5* at the sites of active skeletal growth and *MmpL7* regulates skeletal elongation

Miri Morgulis, Mark R. Winter, Ligal Shternhell, Tsvia Gildor, Smadar Ben-Tabou de-Leon *

Department of Marine Biology, Leon H. Charney School of Marine Sciences, University of Haifa, Haifa, 31905, Israel

ARTICLE INFO

Keywords:
Matrix metalloproteinase
Biomineralization
Sea urchin
Gene regulation
Tubulogenesis
Vascular endothelial growth factor

ABSTRACT

Organisms can uptake minerals, shape them in different forms and generate teeth, skeletons or shells that support and protect them. Mineral uptake, trafficking and nucleation are tightly regulated by the biomineralizing cells through networks of specialized proteins. Specifically, matrix metalloproteases (MMPs) digest various extracellular substrates and allow for mineralization in the vertebrates' teeth and bones, but little is known about their role in invertebrates' systems. The sea urchin embryo provides an excellent invertebrate model for genetic and molecular studies of biomineralization. MMP inhibition prevents the growth of the calcite spicules of the sea urchin larval skeleton, however, the molecular mechanisms and genes that underlie this response are not well understood. Here we study the spatial expression and regulation of two membrane type MMPs that were found to be occluded in the sea urchin spicules, *Pl-MmpL7* and *Pl-MmpL5,* and investigate the function of *Pl-MmpL7* in skeletogenesis. The inhibition of MMPs does not change the volume of the calcium vesicles in the skeletogenic cells. The expression of *Pl-MmpL7* and *Pl-MmpL5* is regulated by the Vascular Endothelial Growth Factor (VEGF) signaling, from the time of skeleton initiation and on. The expression of these genes is localized to the subsets of skeletogenic cells where active spicule growth occurs throughout skeletogenesis. Downregulation of *Pl-MmpL7* expression delays the growth of the skeletal rods and in some cases, strongly perturbs skeletal shape. The localized expression of *Pl-MmpL7* and *Pl-MmpL5* to the active growth zone and the effect of *Pl-MmpL7* perturbations on skeletal growth, suggest that these genes are essential for normal spicule elongation in the sea urchin embryo.

1. Introduction

Biomineralization is the process by which soft organic tissues use minerals to produce shells, skeletons and teeth for various functions such as protection and physical support (Lowenstam and Weiner, 1989). This process occurs within organisms from the five kingdoms of life that utilize about 60 different minerals and shape them in various forms and sizes (Lowenstam and Weiner, 1989). Biomineralization is believed to have evolved independently in different phyla, by the co-option of pre-existing developmental programs and evolution of specialized proteins (Erwin, 2020; Morgulis et al., 2019; Murdock and Donoghue, 2011; Murdock, 2020; Sarashina and Endo, 2006). In many biomineralizing organisms, the minerals are accumulated in an amorphous phase in vesicles and then deposited into a dedicated compartment where crystallization occurs (Mass et al., 2017; Vidavsky et al., 2014, 2015; Weiner and Addadi, 2011). In our bones and teeth, the biomineralization compartment is the extracellular matrix (ECM) secreted from the biomineralizing cells and remodeled by enzymes and proteases (Kawasaki et al., 2009; Reznikov et al., 2016; Weiner and Addadi, 2011; Yoshizaki and Yamada, 2013). The molecular regulation of the ECM in the biomineralization compartment is a key to the mechanistic understanding of the biological control of biomineralization and its evolution.

An important family of proteases that regulates the process of biomineralization in the mammalian teeth and bones is the matrix metalloproteases (MMPs), specifically, MMP9, MMP13, MMP14 and MMP20 (Bourd-Boittin et al., 2005; Kawasaki et al., 2009; Page-McCaw et al., 2007; Yoshizaki and Yamada, 2013). The MMP family is divided into several groups according to the substrate and structure (Page-McCaw et al., 2007; Rundhaug, 2005). Basic type MMPs, such as MMP13 and MMP20, include a signal peptide, a pro-peptide, a catalytic domain and a hemopexin domain (Kim and Joh, 2012; Page-McCaw et al., 2007). In addition to these domains, MMP9 contains a fibronectin domain inserted

* Corresponding author.
E-mail address: sben-tab@univ.haifa.ac.il (S. Ben-Tabou de-Leon).

https://doi.org/10.1016/j.ydbio.2021.01.013
Received 17 September 2020; Received in revised form 26 January 2021; Accepted 27 January 2021
Available online 9 February 2021

into its catalytic domain and MMP14 is a membrane-type MMP that is chained to the cell surface by a transmembrane domain (Page-McCaw et al., 2007; Rundhaug, 2005). These MMPs have numerous roles in regulating the growth of mammalian teeth and bones (Page-McCaw et al., 2007). MMP20 is expressed specifically in ameloblasts and cleaves enamel specific ECM proteins, so they can be replaced by calcium and phosphate during enamel maturation stage (Yoshizaki and Yamada, 2013). The bone elongates by the mineralization of the cartilage mold made by chondrocytes in the growth plate. For the transition from cartilage to bone, the chondrocytes have to go through apoptosis, regulated by MMP9, and collagen degradation by MMP9, MMP13 and MMP14 (Page-McCaw et al., 2007; Vu et al., 1998; Zhou et al., 2009). Thus, MMP9, MMP13, MMP14 and MMP20 degrade various ECM proteins and through this process promote biomineralization in mammalian teeth and bones.

The role of MMPs in mammalian biomineralization makes it interesting to study the role of the homologs of these proteins in the biomineralization of other organisms; this could elucidate the common mechanisms that animals use to shape biominerals. The sea urchin, of the echinoderm phylum, presents an excellent model system to study the role of MMPs in invertebrate biomineralization. The sea urchin embryo is transparent and relatively small (~200 μm at the pluteus stage) which enables the detection of all stages of larval skeletogenesis that occur quite rapidly (2–3 days post-fertilization, [dpf]). Genetic and pharmacological perturbations are easy to conduct in sea urchin embryos allowing the investigation of the molecular control systems in these embryos. These experimental advantages were used to illuminate the pathway of mineral uptake and deposition on the one hand (Beniash et al., 1999; Gibbins et al., 1969; Vidavsky et al., 2014) and on the other hand, to generate one of the most comprehensive models of a developmental gene regulatory network (GRN) (Adomako-Ankomah and Ettensohn, 2013; Ettensohn, 2013; Morgulis et al., 2019; Oliveri et al., 2008; Stepicheva and Song, 2015). For all these reasons, sea urchin larval skeletogenesis is a promising system for investigating the role of MMPs in biomineralization outside the vertebrates' phylum.

Echinoderms are close relatives of vertebrates, yet the biomineralization programs of these two phyla are quite distinct. Echinoderm skeletons are made of Calcium Carbonate rather than Calcium Apatite used in vertebrate biomineralized tissues (Raff and Byrne, 2006). The biomineralization compartment in echinoderm is an internal cavity generated by a syncytium of skeletogenic cells (Ettensohn, 2013; Morgulis et al., 2019; Oliveri et al., 2008). The larval skeleton of the sea urchin is made of two rods of calcite, the spicules (Ettensohn, 2013). To produce the spicules, the skeletogenic cells accumulate calcium and carbon through endocytosis and concentrate them in the form of amorphous calcium-carbonate (ACC) in intracellular vesicles (Vidavsky et al., 2014, 2015, 2016; Wilt et al., 2008). The ACC carrying vesicles are then secreted into the spicule syncytial cord where crystallization occurs (Beniash et al., 1999; Ingersoll and Wilt, 1998; Killian and Wilt, 2017; Vidavsky et al., 2014; Winter et al., 2020). Crystallization is regulated by specialized matrix proteins that are secreted into the spicule cavity and then become a part of the forming spicule (Mann et al., 2010b). A proteomic analysis of the proteins occluded in the calcite spicules identified three key groups of proteins, lectin-like matrix proteins (*e.g.*, SM50 and SM30), membrane bound glycoproteins and MMPs (Mann et al., 2010b). The roles of some of these proteins were studied and they were found to be important for different aspects of biomineralization. For example, the spicule matrix protein, SM50, stabilizes the amorphous phase of the calcium carbonate and delays crystallization (Mao et al., 2016; Rao et al., 2013). Thus, specialized proteins, including MMPs, operate in the spicule cord of the sea urchin embryo and deciphering their function could elucidate the regulation of biomineralization in this important model system.

Five genes that encode sea urchin MMPs are found occluded in the spicules: MmpL8/19 (basic type), MmpL2 (homolog to vertebrates' MT5-MMP), MmpL5, MmpL6 and MmpL7 (homologs to vertebrates' MT1-4 MMP) (Mann et al., 2010b). The last four are also present in the test, spine and tooth of the adult sea urchin, suggesting that they participate in the biomineralization process even after the embryonic stage (Mann et al., 2010a, 2010b). The expression of the genes, *MmpL2* and *MmpL6* was studied at the gastrula stage in the sea urchin, *Strongylocentrotus purpuratus* (*S. purpuratus)* and was found to be localized in the skeletogenic lateral cell clusters, where the spicules are generated at this time (Sun and Ettensohn, 2014). The function of specific MMP genes has not been studied before, however, the inhibition of all MMPs by the inhibitor Batimastat (BB94), completely blocks skeletal growth (Ingersoll et al., 2003; Ingersoll and Wilt, 1998). In this condition, the skeletogenic cells still fuse and form the first calcite granule, but the spicules do not grow beyond this granule (Ingersoll et al., 2003; Ingersoll and Wilt, 1998). Scanning electron microscope (SEM) examination of a culture of skeletogenic cells grown under MMP inhibition shows the accumulation of vesicle with unidentified content in the cytoplasm of the spicules (Ingersoll et al., 2003; Ingersoll and Wilt, 1998). Overall, five MMPs are present in the sea urchin spicules and MMPs inhibition prevents skeletal growth, however, the regulation of the sea urchin MMPs and the mechanisms through which they affect biomineralization, are largely unknown.

A key regulator of sea urchin spiculogenesis is the Vascular Endothelial Growth Factor (VEGF) pathway (Adomako-Ankomah and Ettensohn, 2013; Duloquin et al., 2007), which controls blood vessel formation in vertebrates (Potente et al., 2011). The inhibition of sea urchin VEGF signaling completely abolishes skeleton formation (Adomako-Ankomah and Ettensohn, 2013; Duloquin et al., 2007). We recently studied the cellular and molecular machinery activated by the VEGF pathway during sea urchin skeletogenesis and revealed multiple parallels to the regulation of vertebrate vascularization (Morgulis et al., 2019). This similarity and the participation of VEGF signaling in generating tubular structures in various phyla led us to propose that the biomineralization program in echinoderms was co-opted from an ancestral tubulogenesis program, from which vertebrates' vascularization evolved (Morgulis et al., 2019).

Among the hundreds of genes that respond to VEGFR inhibition, we identified the MMPs, *Pl-MmpL7* and *Pl-MmpL5*, that encode two of the most abundant MMPs found occluded in the sea urchin larval spicules (Mann et al., 2010b). Both genes are homologs of the vertebrates' membrane type MMPs, MMP14 and MMP16. As mentioned above, MMP14 plays a role in vertebrate bone remodeling through its digestion of the collagenous cartilage that enables bone mineralization (Holmbeck et al., 2003; Zhou et al., 2009). To better understand the role of MMPs in sea urchin skeletogenesis, here we examine the effect of MMP inhibition on calcium vesicle volume in the sea urchin embryos using lattice light sheet microscopy (Winter et al., 2020). We study the spatio-temporal expression and regulation by VEGF signaling of *Pl-MmpL7* and *Pl-MmpL5* and investigate the role of *Pl-MmpL7* in spicule elongation. Our results support a prominent role of Pl-MmpL7 and Pl-MmpL5 in sea urchin skeletogenesis.

2. Material and methods

2.1. Animal and embryo cultures

This study was done in two different locations and therefore we used two different sea urchin species that were locally available for research, the Atlantic species, *Lytechinus variegatus* (*L. variegatus*) and the Mediterranean species *Paracentrotus lividus* (*P. lividus*). These species shared a common ancestor about 50 million years ago but their gene regulatory networks and overall skeletal morphology are quite similar. Prominently, both species show similar skeletal perturbation in response to VEGFR inhibition (Adomako-Ankomah and Ettensohn, 2013; Morgulis et al., 2019).

Adult *L. variegatus* were obtained from the Duke University Marine Laboratory (Beaufort, NC, USA). Spawning was induced by intracoelomic injection of 0.5M KCl. Embryos were cultured in artificial sea water at 23

°C. Adult *P. lividus* were obtained from the Institute of Oceanographic and Limnological Research (IOLR) in Eilat, Israel. They were then kept in aquaria located in a dedicated room, raised in 36 ppt in artificial sea water (ASW). Eggs and sperm were obtained by injecting adult sea urchin with 1 ml of 0.5M KCl. Embryos were cultured at 18 °C in 0.2μ filtered ASW.

2.2. Batimastat (BB94) treatment

L. variegatus embryos were cultured with 5 μM of the metalloproteinase inhibitor BB94 (APExBio Cat# A2577) from 11hpf and on. BB94 was melted in DMSO and then diluted in artificial sea water.

2.3. Calcein staining

A 2 mg/ml stock solution of green calcein (C0875, Sigma, Japan) was prepared by dissolving the chemical in distilled water. Working solution of 25 μg/ml was prepared by diluting the stock solution in artificial sea water. *L. variegatus* embryos were grown in calcein artificial sea water from fertilization and washed from calcein about two to 3 h prior to the experiments.

2.4. FM4-64 staining

A 100 μg/ml stock solution of FM4-64 (T13320, Life technologies, OR, USA) was prepared by dissolving the chemical in distilled water. Working solution of 5 μg/ml was prepared by diluting the stock solution in artificial sea water. *L. variegatus* embryos were immersed in working solution about 10 min before visualization.

2.5. Sample preparation for lattice light sheet microscopy

2% low melting agarose (Sigma cat# A0701) melted in artificial sea water at 37 °C was added to the stained embryos at the ratio of 5:1, to immobilize the embryos. The sample was then immersed in the microscope tab with 8 mL artificial sea water with 20 μL FM4-64 working solution.

2.6. Lattice light sheet microscopy

The lattice light sheet microscope (LLSM) used in these experiments is housed in the Advanced Imaged Center (AIC) at the Howard Hughes Medical Institute Janelia research campus (Winter et al., 2020). The system is configured and operated as previously described (Chen et al., 2014; Winter et al., 2020). Samples are illuminated by a 2D optical lattice generated by a spatial light modulator (SLM, Fourth Dimension Displays). The sample is excited by 488 nm, diode lasers (MPB Communications) at 30 mW through an excitation objective (Special Optics, 0.65 NA, 3.74-mm WD). Fluorescent emission is collected by detection objective (Nikon, CFI Apo LWD 25XW, 1.1 NA), and detected by a sCMOS camera (Hamamatsu Orca Flash 4.0 v2). Acquired data are deskewed as previously described (Chen et al., 2014) and deconvolved using an iterative Richardson-Lucy algorithm with a point-spread function inferred for the lattice-light sheet optical system.

2.7. Rendering, segmentation and quantification of vesicle volume

To visualize the 3D structure and motion of the cells and the vesicles in the embryos throughout time (rendering), we reconstructed a 3D model from the individual slices and then connected these images over time to produce time-lapse sequences, visualized using the LEVER software (Winter et al., 2016). The automatic detection of vesicles in each frame (segmentation) is accomplished using the high-performance Hydra Image Processing library for fast 3-D image filtering (Wait et al., 2019). We use a blob-detection approach similar to Chenourd et al. based on the Laplacian of Gaussians (LOG) filter (Chenouard et al., 2014). The LOG filter can be used for blob-like object detection. In this work we used a thresholded 3D LOG to identify the vesicles in each frame. This method identifies the size and position of each vesicle. Source code for all segmentation and statistical analyses can be found in the GitLab repository: https://git-bioimage.coe.drexel.edu/opensource/llsm-calcium-vesicles-lever.

2.8. Statistical analysis of vesicle volume

We used nine control and eleven metalloproteinase inhibited time-lapses for the analysis. The details of the time-lapses and number of vesicles measured in each movie is provided in Dataset S1. For the analysis of differences in median vesicle volume, we first apply the Kruskal-Wallis one-way rank test to identify if there are significant differences across all experimental groups and regions (Winter et al., 2020). If a significant difference is observed, then post-hoc pairwise analysis (Dunn-Sidak) is carried out between groups to identify differences between each pair of interest. The MATLAB version 2019b software package was used to perform the analysis. The p-values of each comparison are presented in Dataset S1.

2.9. Axitinib (AG013736) treatment

Axitinib treatment was done in *P. lividus* embryos. A 5 mM stock solution of the VEGFR inhibitor, axitinib (AG013736, Selleckchem, Houston, TX, USA), was prepared by reconstituting this chemical in dimethylsulfoxyde (DMSO). The axitinib stock was diluted in ASW to a final concentration of 150 nM of working solution. Control embryos in all experiments were cultured in equivalent concentrations of 0.1% DMSO (v/v).

2.10. Imaging

All the embryos images presented in Figs. 3–5 were acquired using Ziess Axioimager M2.

2.11. QPCR expression level quantification

Total RNA was extracted from >1000 *P. lividus* embryos in each time point using RNeasy Mini Kit (50) from QIAGEN (#74104) according to the kit protocol using DNase treatment from RNease-Free DNase Set-Qiagen (50) (#79254). 1 μg of total RNAs were reverse-transcribed using the High Capacity cDNA RT kit, AB-4368814 (Applied Biosystems) following the manufacturer's instructions. QPCR was carried out in triplicates as described before (Morgulis et al., 2019). Primer sets for the genes were designed using Primer3Plus (http://www.bioinformatics.nl/cgi-bin/primer3plus/primer3plus.cgi/): Pl-MmpL5-QF 5- CAATCGCAAAGTTCAAGCAA-3; Pl-MmpL5-QR 5-CAGCCTCCCTTAGCTCTTCA-3; Pl-MmpL7-QF 5-TCGTACTGGTGGTCGTGTTA-3; Pl-MmpL7-QR 5-ATACGGGTGTTGGGATCGTT-3. The quantification of the relative levels of mRNA per sample and the calculation of gene initiation times were done as described in (Gildor and Ben-Tabou de- Leon, 2015).

2.12. Whole mount in-situ hybridization (WMISH)

Total RNA of 30hpf *P. lividus* embryos was used to generate cDNA using the High capacity cDNA RT AB-4368814 (Applied Biosystems). cDNAs of the tested genes were PCR amplified, using the following primers: Pl-MmpL5-F 5-GGCTCATTCTGACGTGAGT-3; Pl-MmpL5-R 5-CACAATAATTATCCAAAGCATAAAGTAATTTC-3; Pl-MmpL7-F 5-GAACTTGGCAAAGTTTGACTGAACTTC-3; Pl-MmpL7-R 5- CAATGAATGTCGAATGGGAGGTTATTG -3. The PCR fragments were ligated and inserted into pGemT (Promega A3600). RNA DIG probes were generated using ROCHE DIG labeling kit (catalog number 1277073910) and SP6 polymerase 10810274001 sigma. WMISH was performed as described in (Morgulis et al., 2019).

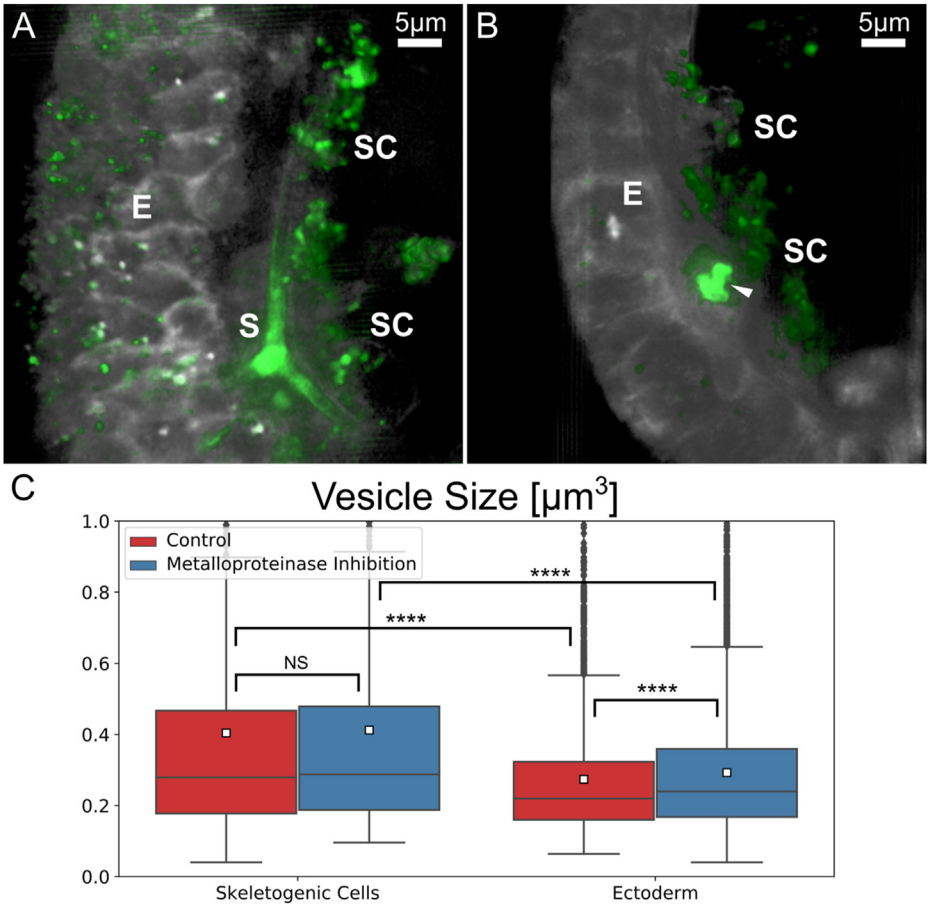

Fig. 1. Inhibition of metalloprotease activity does not affect calcium vesicle volume in the skeletogenic mesodermal cells. (A–B) Examples of the LLSM 3D images of sea urchin embryos in control (A) and under metalloproteinase inhibition (B). These representative images are the first 3D rendered frames of selected datasets. Calcein staining is marked in green and the FM4-64 membrane staining is marked in gray. The embryo that was treated with the metalloproteinase inhibitor, BB94, shows a small calcium grain that doesn't grow (arrowhead in B) compared to the elongated spicule in the control embryo (marked S, in A). E – ectoderm, S - spicule, SC – skeletogenic cells. Scale bars are 5 μm. 3D movies showing the first 100–200 frames of each of the datasets presented in (A) and (B) are provided as Supplementary Videos S1–S2. (C) Comparison of vesicle volumes in the ectoderm and in the skeletogenic cells in control and under metalloproteinase inhibition. Each box plot shows the average (white square) median (middle line), the first and the third quartiles (the 25th and 75th percentiles, edges of boxes) and outliers (black diamonds). (Standard *t*-test, **** indicates $p < 0.0001$, exact p-values are given in Dataset S1). The total number of vesicles measured in the control skeletogenic cells: 815, ectodermal cells: 3719; Metalloproteinase inhibition skeletogenic cells: 1072, ectodermal cells: 6941.

2.13. Morpholino antisense oligonucleotides (MASO) microinjections

Translation or splicing of *Pl-MmpL7* was blocked by the microinjection of *Pl-MmpL7* MASO into sea urchin eggs. MASO was synthesized (Gene Tools, Philomath, OR) complementary to the sequence of *Pl-MmpL7* mRNA: 5- CGACACCAGCATAGACCGTCATCAT-3 (translation) and to the junction between the third exon and the fourth intron: 5-TCTGGGATTGGATGATTAGAAATGA-3 (splicing). The injection of the splicing MASO generated a deletion of the fourth exon that contains the peptidase domain, as tested by PCR of cDNA prepared from injected embryos (Fig. S2). Microinjection solutions were prepared containing 800 μM *Pl-MmpL7* MASO, 0.12 M KCl and 1 μg/ml Rhodamine Dextran. Embryos injected with similar concentration of random MASO were used as a control. Three biological replicates (different pairs of parents) were studied at 72hpf. At each biological replicate in each condition 36–59 embryos were scored for phenotypes.

2.14. PCR of splicing MASO injections

About 150 injected or uninjected embryos were collected at 40hpf and mRNA was extracted using RNeasy Micro Kit (50) from QIAGEN (#74004) according to the kit protocol using DNase treatment from RNease-Free DNase Set- Qiagen (50) (#79254). Reverse-transcription was done using the High Capacity cDNA RT kit, AB-4368814 (Applied Biosystems) following the manufacturer's instructions. PCR was then conducted using the 5x HOT FIREPol Blend MM RLT 7.5 (Solis Biodyne, 04-25-00115) and the following primers: *PlMmpL7*-Exon3-F1 5-CGTATGTCCCTGATAGCCCA-3; *PlMmpL7*-Exon5-R1 5-AATGGAGCCATGAGGGCGC-3. PCR fragment were then run of a gel and demonstrated the normal and truncated *Pl-MmpL7* transcripts (Fig. S2).

2.15. Statistical analysis of rods length in the MASO experiments

The length of the rods at 72hpf was manually measured using the ImageJ software using the straight line tool. The measurements were repeated for three biological replicates with a total of 40–42 rods being measured for each condition. Statistical analyses were done using IBM SPSS statistics 21. Post-oral rods length measurements (μm) exhibiting a skewed distribution were transformed, using the natural logarithms to satisfy the prerequisite assumptions of normality by Kolmogorov-Smirnov test. Then, One-Way ANOVA test was conducted following by Bonferroni post hoc analysis. Body rods length measurements were not normally distributed even after several transformations. Therefore, a Kruskal-Walis a-parametric test, which is equivalent of a one-way ANOVA was performed. The body and post-oral rods means were compared for each treatment (Random, Translation and Splicing MASO) generating the following results: Post-oral rods Random MASO ($M = 193.3$, $SD = 3.9$), Translation MASO ($M = 93.5$, $SD = 5.6$), Splicing MASO ($M = 97.3$, $SD = 7.5$); $F_{2,121}(P < 0.0001, R2 = 0.504)$. Body rods Random MASO ($M = 231.2$, $SD = 3.3$), Translation MASO ($M = 162.5$, $SD = 4.4$), Splicing MO ($M = 155.2$, $SD = 4.3$); $chi^2 = 57.8$, $P < 0.0001$, $df = 1$.

3. Results

3.1. MMP inhibition does not affect calcium vesicle volume in the sea urchin embryo

Previous studies of the effect of MMP inhibition using BB94, a potent, broad inhibitor of MMP activity, showed an accumulation of vesicles in the skeletogenic cells, that were interpreted as yolk granules (Ingersoll et al., 2003; Ingersoll and Wilt, 1998). The importance of calcium vesicles

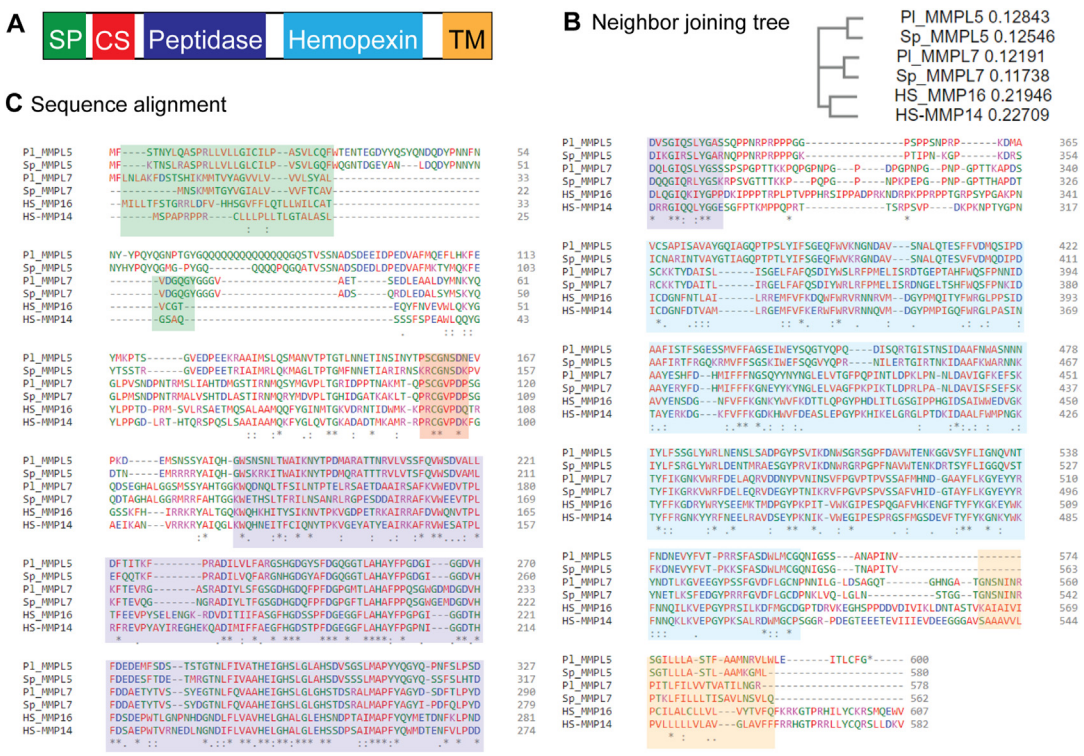

Fig. 2. Basic structural domains are conserved between human MT-MMPs and sea urchin *MmpL5* and *MmpL7*. (A) Diagram showing the functional domains in the human protein MMP14 (MT1-MMP) and MMP16 (MT3-MMP) protein sequences. (B) Neighbor-joining tree of human MMP14, MMP16 and the sea urchin genes, using clustal omega showing unrooted tree. (C) Alignment of the sea urchin MmpL5 and MmpL7 of *S. purpuratus* and *P. lividus* and the human MMP14 and MMP16 by clustal omega. The colors represent the structural domains of the MMP proteins. Asterisk indicates amino acid identity, highly similar amino acids are indicated in two dots and similar amino acids are indicated in one dot.

in the process of biomineralization makes it intriguing to study the effect of MMP inhibition on the volume of calcium vesicles in the sea urchin cells. We recently used calcein staining and lattice light sheet microscopy (LLSM) to study the 3D volume and kinetics of calcium bearing vesicles in the sea urchin embryo in control and under VEGFR inhibition (Winter et al., 2020). LLSM produces high spatial and temporal resolution images, while avoiding the phototoxicity problems that are common with confocal and standard LSM (Chen et al., 2014). Calcein binds alkaline divalent ions, including calcium, and was used before to track calcium bearing vesicles in the sea urchin embryo (Gildor et al., 2019; Vidavsky et al., 2014). We detected an increase in the volume of calcein-stained vesicles in both the skeletogenic and ectodermal cells under VEGFR inhibition, possibly, since calcium is accumulated in the blastocoel to higher levels when the spicule is not made. In the same set of experiments, we studied the volume of calcein-stained vesicles under MMP inhibition, using BB94, and we present the results here. Details of the time-lapses we used in this work are provided in Dataset S1.

We use calcein to stain calcium (Vidavsky et al., 2014) and FM4-64 to mark cell membranes in live sea urchin embryos of the species, *L. variegatus*, during skeletogenesis (Fig. 1A and B) (Morgulis et al., 2019; Winter et al., 2020). We reconstruct a 3D model to visualize the 3D structure and motion of the cells and the vesicles in the embryos through time (Winter et al., 2020). Representative movies are provided (supplementary movies S1, control, and S2, BB94) and the first frame of these movies is presented in Fig. 1A (control) and B (BB94). When the MMPs are inhibited, the spicules do not grow beyond a small granule (Arrowhead in Fig. 1B compared to the elongated spicule in Fig. 1A(, in agreement with previous studies (Ingersoll et al., 2003; Ingersoll and Wilt, 1998). We automatically quantify vesicle volume, using a segmentation algorithm as described in (Winter et al., 2020). We differentiate between the skeletogenic mesodermal cells and the other territories manually in the first frame of each movie and use this frame for volume statistics (Fig. 1C).

Supplementary data related to this article can be found at https://doi.org/10.1016/j.ydbio.2021.01.013.

The median volume of calcein stained vesicles in the skeletogenic mesodermal cells does not change due to the BB94 treatment, but it mildly increases in the ectoderm under this condition (Fig. 1C, Dataset S2). The median vesicle volume in the skeletogenic mesodermal cells is significantly larger than in the ectodermal cells in both control and MMP inhibition (Fig. 1C, Dataset S1). This difference indicates different calcium processing by the cells of the two tissues in agreement with previous studies (Kahil et al., 2020; Vidavsky et al., 2016; Winter et al., 2020). The small increase in the volume of the ectodermal calcium vesicles under MMP inhibition could be due to the increased calcium level in the blastocoel since calcium is not sequestered into the spicules in this condition. The lack of effect on calcium vesicles volume in the skeletogenic mesodermal cells suggests that the MMPs are not involved in calcium vesicle endocytosis or deposition, and the strong effect of the MMP inhibition is probably due to other biomineralization related processes.

The membrane type MMPs, *Pl-MmpL5* and *Pl-MmpL7,* are activated by VEGF signaling at the lateral skeletogenic clusters at the time of spicule formation.

In a previous study we identified hundreds of genes that respond to VEGFR inhibition, among them the MMPs, *Pl- MmpL5* and *Pl- MmpL7* (Morgulis et al., 2019). The proteins encoded by these genes are of the most abundant proteins found in the calcite spicule of the sea urchin, *Strongylocentrotus purpuratus* (*S. purpuratus*) (Mann et al., 2010b). The best blast hits to both *Pl-MmpL5* and *Pl-MmpL7* in the human genome are the membrane type MMPs, MMP14 and MMP16 (Fig. 2). As mentioned above, MMP14 participates in bone remodeling in mammals (Holmbeck et al., 2003; Zhou et al., 2009). Interestingly, it is activated by VEGF signaling in endothelial cells and is required for vascular tubulogenesis (Hanjaya-Putra et al., 2010; Sacharidou et al., 2010; Stratman et al.,

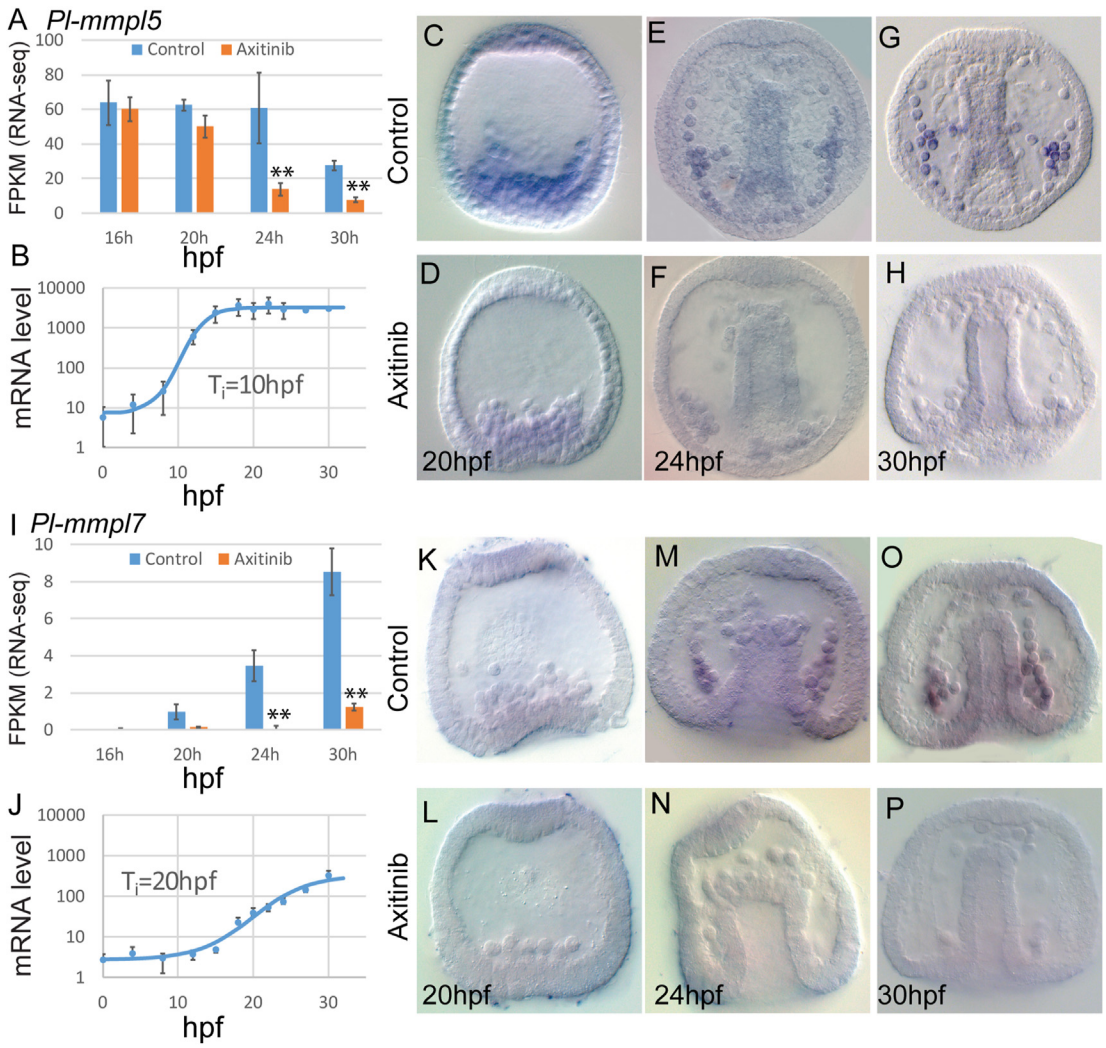

Fig. 3. *Pl-MmpL5* and *Pl-MmpL7* spatio-temporal expression and regulation by VEGF signaling during early skeletogenesis. We present the following data for *Pl-MmpL5* and *Pl-MmpL7,* respectively: (A, I) Gene expression level for control and VEGFR inhibited embryos measured by RNA-seq in Fragments Per Kilobase of transcript per Million mapped reads (FPKM, asterisks indicate FDR<0.05, 16hpf and 20hpf, n = 2, 24hpf and 30hpf, n = 4, see (Morgulis et al., 2019) for details); (B, J) Temporal expression profile and expression initiation time, T_i (QPCR, n = 3, error bars correspond to standard deviation.); (C–H, K–P) spatial gene expression in control and in VEGFR inhibited embryos at 20hpf (C,D, K,L), 24 (E,F,M,N) and 30hpf (G,H,O,P). The whole-mount in-situ hybridization experiments were repeated in three independent biological replicates where at each condition at least 30 embryos were scored.

2009). Sequence comparison with the human proteins indicates that there are conserved functional domains within the sea urchin MMP proteins, including: signal peptide, pro-domain (cysteine switch), catalytic domain (peptidase), hemopexin and transmembrane domain (Fig. 2). Hence, based on the sequence homology of *Pl-MmpL5* and *Pl-MmpL7* to mammalian MMP14, they could have a role in both sea urchin biomineralization and tubular spicule formation.

To further understand the expression pattern of *Pl-MmpL5* and *Pl-MmpL7* and to verify their transcriptional response to VEGF signaling we studied their spatio-temporal expression and response to VEGFR inhibition during the early stages of skeletogenesis (Fig. 3). *Pl-MmpL5* is activated at the blastula stage (10hpf, Fig. 3B) in the skeletogenic cells (Fig. 3C), and its expression is independent of VEGF-signaling up to 20hpf (Fig. 3A). However, at 24hpf, *Pl-MmpL5* expression becomes dependent on VEGF signaling and decreases significantly when VEGFR is inhibited (see Fig. 3A and compare 3E and 3F). At this time and at 30hpf, *Pl-MmpL5* expression is localized to the skeletogenic lateral cell clusters where spicule formation is initiated (Fig. 3G and H). *Pl-MmpL7* turns on at the beginning of gastrulation (~20hpf, Fig. 3J), it is detected at the skeletogenic lateral cell clusters from 24hpf and on (Fig. 3M, O) and its expression depends on VEGF signaling (Fig. 3I, N, P). Thus, the membrane type MMPs, *Pl-MmpL5* and *Pl-MmpL7*, are expressed in the skeletogenic cells and their expression in the skeletogenic cell clusters depends on VEGF signaling during the first stages of spicule formation.

Pl-MmpL5 and *Pl-MmpL7* are expressed at the tips of the growing rods and are regulated by VEGF signaling in the post-oral and anterolateral rods.

We wanted to study the expression of *Pl-MmpL5* and *Pl-MmpL7* and their regulation by VEGF in the pluteus stage, when the spicules elongate and form the different skeletal rods. At these stages of skeletogenesis, the body, anterolateral and post-oral rods grow rapidly at their tips and slowly at their girth, suggesting that calcium deposition is restricted to the growing tips and inhibited elsewhere (Fig. 4A (Sun and Ettensohn, 2014),). At this time, VEGF is expressed only in the ectodermal cells near the tips of the post-oral and anterolateral rods and not near the tips of the body rods (Adomako-Ankomah and Ettensohn, 2013; Duloquin et al., 2007). Accordingly, VEGFR continuous inhibition completely blocks skeletogenesis up to the pluteus stage (Fig. 4B), while the addition of VEGFR inhibitor after the gastrula stage (~25hpd in *P. lividus*), inhibits only the growth of the anterolateral and post-oral rods and doesn't affect the growth of the body rods (Fig. 4C (Sun and Ettensohn, 2014),). We wanted to test in which cells *Pl-MmpL5* and *Pl-MmpL7* are expressed in

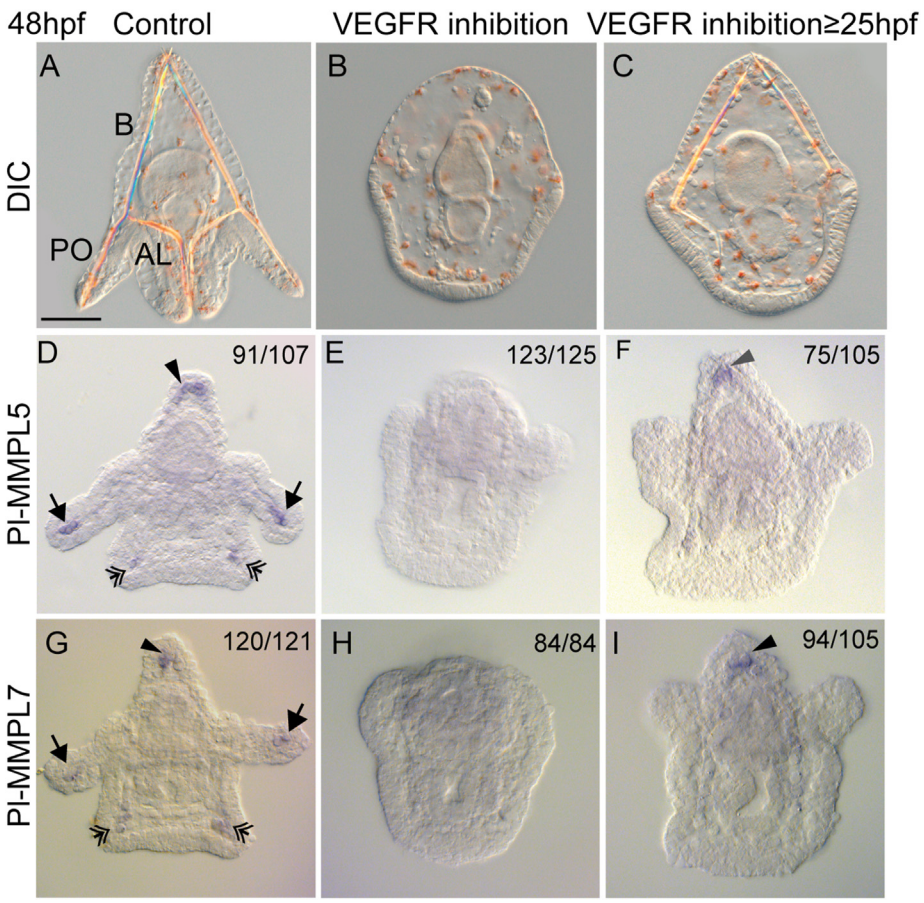

Fig. 4. *Pl-MmpL5* and *Pl-MmpL7* are expressed at the tip of the growing rods and depend on VEGF signaling at 48hpf. Embryos were grown in control (left panels), continuous VEGFR inhibition (middle panels) and addition of VEGFR inhibitor at 25hpf (right panels). (A–C) Representative live embryos in the three experimental conditions at 48hpf. B – body rods, AL – anterolateral rods, PO - post-oral rods. (D–I) Spatial expression (WMISH results) of *Pl-MmpL5* and *Pl-MmpL7* in the three experimental conditions at 48hpf. Both genes are expressed in the cells at the tips of the body rods (arrowheads), the anterolateral rods (double arrows) and the post-oral rods (arrows, D, G). The expression of both genes is completely downregulated by continuous inhibition of VEGFR (E, H). The addition of VEGFR inhibitor at 25hpf downregulated the expression of the two genes at the post-oral and anterolateral rods but not at the tip of the body rods (F, I). The numbers shown at the top-right of each image state the number of embryos that show this expression pattern out of all embryos scored, based on three independent biological replicates.

the pluteus stage and whether these genes are still regulated by VEGF signaling.

The expression of *Pl-MmpL5* and *Pl-MmpL7* is detected at the tips of the body, anterolateral and post-oral rods, at the pluteus stage (48hpf, Fig. 4D, G, and 40hpf, Figs. S1A and D). Continuous inhibition of VEGFR completely eliminates the expression of the two genes in the pluteus stage (48hpf, Fig. 4E, H, and 40hpf, Figs. S1B and E). However, the addition of VEGFR inhibitor at the gastrula stage, reduces the expression of *Pl-MmpL5* and *Pl-MmpL7* only in the cells at the tips of the post-oral and anterolateral rods, but not in the cells at the tips of the body rods (48hpf, Fig. 4F, I, and 40hpf, Figs. S1C and F). Thus, during skeletal elongation, *Pl-MmpL5* and *Pl-MmpL7* are expressed in the skeletogenic cells localized at the tips of the growing rods, where rapid extension of the spicule occurs, and their expression in the tips of the post-oral and anterolateral rods, depends on VEGF signaling.

3.2. *Downregulation of Pl-MmpL7 induces severe delays in spicule elongation*

The gene *Pl-MmpL7* is turned-on by VEGF signaling when spicule formation starts (Fig. 3I-P) which could imply that this gene has an important role in the elongation of the spicules. We therefore downregulated the expression of this gene in sea urchin embryos and observed the skeletogenic phenotypes. We knocked-down *Pl-MmpL7* expression by microinjection of two specific morpholino antisense oligonucleotides (MASOs) into sea urchin eggs, one that blocks translation and one that prevents splicing (Fig. S2A). Specifically, the splicing MASO was expected to prevent the splicing of the fourth exon that contains most of the catalytic domain, thereby eliminating this domain from the mature mRNA transcripts (Fig. S2B). We verified that the splicing MASO was effective using PCR of the respective region on cDNA extracted from injected embryos, using random MASO as a control (Fig. S2C).

At 72hpf, all the rods of the spicules are elongated in control embryos (Fig. 5A) while embryos injected with *Pl-MmpL7* translation or splicing MASO show delays in the elongation of all the spicule rods (Fig. 5B and C). In some embryos, the tips of the post-oral rods show extra branching but this was also observed in embryos injected with random MASO (Fig. 5B). In a minority of the *Pl-MmpL7* morphant embryos we observe a severely disrupted skeletal structure (Fig. 5C). A summary of the different phenotypes is presented in Fig. 5D. We quantified the length of the post-oral and body rods in embryos injected with random MASO and in *Pl-MmpL7* morphants (Fig. 4E). The measurements show a significant reduction in the length of the post-oral and body rods in both translation and splicing *Pl-MmpL7* MASO compared to control embryos injected with random MASO. Overall, perturbing the expression of *Pl-MmpL7* results with a significant reduction of the growth of the spicule rods, indicating that this protein is important for normal spicule elongation.

4. Discussion

MMPs are major regulators of biomineralization during vertebrates' bone and teeth formation (Bourd-Boittin et al., 2005; Kawasaki et al., 2009; Page-McCaw et al., 2007; Yoshizaki and Yamada, 2013). Deciphering their function in other model organisms can promote our understanding of the molecular control and evolution of biomineralization. Here, we study the role of MMPs in regulating the volume of calcium vesicles and investigate the expression and regulation of *Pl-MmpL5* and *Pl-MmpL7* in the sea urchin embryo. We perturb the expression of *Pl-MmpL7* and characterize its skeletogenic phenotypes. Our studies reveal the dynamic expression pattern of these genes and shed light on the possible role of MMPs in sea urchin skeletogenesis.

The inhibition of MMP activity using BB94 prevents the elongation of

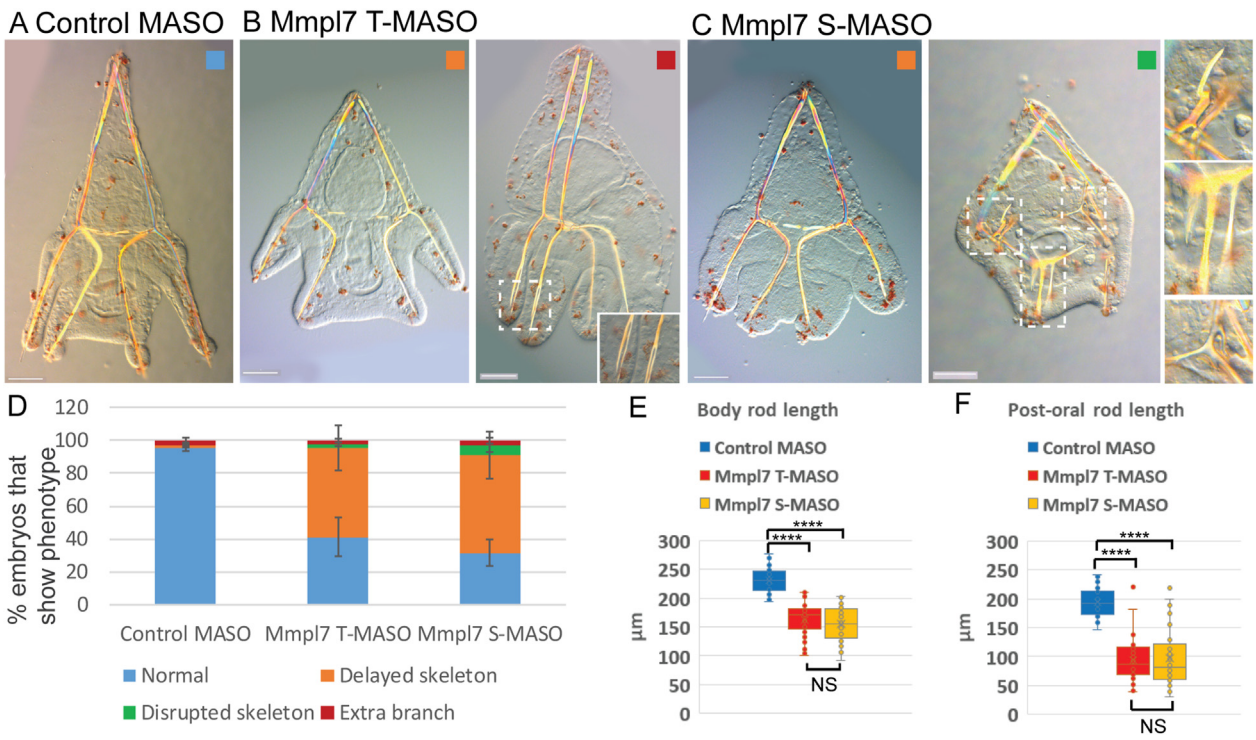

Fig. 5. Downregulation of *Pl-MmpL7* induces severe delays in spicule elongation and disrupts skeletogenesis. (A–C) Representative embryos showing the results of *Pl-MmpL7* knock-down by translation (T-MASO) and splicing (S-MASO) morpholinos at 72 h post fertilization (hpf). (A) Embryo injected with control MASO shows normal skeleton. (B) embryos injected with *Pl-MmpL7* T-MASO show a delayed skeleton phenotype (left) or extra branching phenotype (right). C, embryos injected with *Pl-MmpL7* S-MASO show delayed skeleton (left) or disrupted skeleton (right). High magnifications of the area that are marked with dashed rectangles are presented on the right. (D) Quantification of skeletogenic phenotypes of *Pl-MmpL7* morphants at 72hpf. Color code is indicated in the representative images. Error bars indicate standard deviation of three independent biological replicates where at least 36 embryos were scored for each condition, specifically, n = 118 for control, n = 150 for MmpL7 T-MASO and n = 134 for MmpL7 S-MASO. (E–F) Effect of MmpL7 knock-down on the length of the body rod (E) and the post-oral rod (F). Each box plot shows the median (middle line), the first and the third quartiles (the 25th and 75th percentiles, edges of boxes) and outliers. Based on three biological replicates. **** indicates $p < 0.0001$ in the respective test, NS – not significant, see methods for further details.

the spicules, yet, the volume of the calcium bearing vesicles in the skeletogenic cells is unaffected in this condition (Fig. 1). This finding excludes a major role of the MMPs in calcium vesicle accumulation and secretion, and suggests that the MMP's activity is related to other biomineralization related processes. Based on the role of MMP in mammalian calcification, sea urchin MMPs could be digesting spicule matrix proteins and regulating their maturation and by that promoting biomineralization. Previous studies had shown that the matrix protein SM50 is secreted to the spicule syncytial cord before calcium crystallization occurs (Urry et al., 2000), and that the knock-down of this protein prevents skeletal growth (Peled-Kamar et al., 2002). These findings support the role of spicule matrix proteins in generating a mold for biomineralization that needs to be processed by MMPs before calcification. Nevertheless, SM50 has a single isoform in the spicules that is not cleaved in either control or MMP inhibition embryos (Ingersoll et al., 2003); therefore, SM50 is unlikely to be MMP target. MMP inhibition prevents the processing of the spicule matrix protein, SM30, as only its heavier isoform (46kD) is detected in the spicules in this condition while both the heavy and the light (43kD) isoforms are detected in control spicules (Ingersoll et al., 2003; Ingersoll and Wilt, 1998). However, the knock-down of SM30 did not affect larval skeleton formation (Wilt et al., 2013), and therefore the prevention of SM30 cleavage cannot explain the strong phenotype of MMP inhibition (Fig. 1). Further studies are necessary to reveal the substrates of MMPs catalytic activity that underlie the arrest of spicule growth when they are inhibited.

Pl-MmpL5 and *Pl-MmpL7* encode two of the most abundant MMPs found in sea urchin spicules, test, spine and teeth of (Mann et al., 2010a, 2010b) and here we show that these genes are expressed in the active skeletal growth zones, throughout skeletogenesis (Fig. 3 and 4). *Pl-MmpL5* and *Pl-MmpL7* are expressed in the lateral skeletogenic cell clusters when the spicules start growing there (Fig. 3E, G, M, O) and their expression requires VEGF signaling (Fig, 3F, H, N, P). As the skeleton grows, these two genes are expressed at the tips of the growing body, anterolateral and post-oral rods, the sites of active spicule elongation (Fig. 4D, G, S1A, D). At this time, only their expression at the post-oral and anterolateral rods is dependent on VEGF signaling (Fig. 4F, I, S1 C, F). The expression of *Pl-MmpL5* and *Pl-MmpL7* at the tips of the body rods is unchanged under VEGFR inhibition, indicating that the genes are controlled by another regulatory mechanism there (Fig. 4F, I, S1C, F). Interestingly, the genes that encode most abundant spicule matrix proteins, *e.g.,* SM30 and SM50, show similar expression pattern at the tips of the growing rods that depends on VEGF signaling only in the post-oral and anterolateral rods (Sun and Ettensohn, 2014). The high correlation in the spatial expression and regulation of the MMPs and the matrix proteins further implies that the molecular interactions between them could be essential for biomineralization. Possibly, the matrix proteins are first secreted into the spicule cavity to regulate the mineral phase, and the remodeling of the matrix proteins by Pl-MmpL5 and Pl-MmpL7 promotes calcification.

Knock-down of membrane type MMP, *Pl-MmpL7*, significantly delays spicule elongation (Fig. 5), which is quite remarkable, considering the three other MT-MMPs that are still present in the skeletogenic cells (Fig. 3 and 4 (Sun and Ettensohn, 2014)). The effect of Pl-MmpL7 perturbation could be due to a specific substrate this protein digests or due to the reduction of the overall level of proteases at the spicule front end. Interestingly, a mammalian homolog of Pl-MmpL7, MT1-MMP (MMP14), is critical for both, mineralization in bones (Holmbeck et al., 2003) and tubulogenesis of blood vessels (Sacharidou et al., 2010;

Stratman et al., 2009): MT1-MMP regulates the apoptosis of chondrocytes and the remodeling of unmineralized cartilage that are necessary for postnatal skeletal remodeling in mammals (Holmbeck et al., 2003). MT1-MMP is also activated by VEGF in endothelial cells and its proteolytic activity is necessary for lumen formation and the initiation of tube morphogenesis during vertebrates' vascularization (Hanjaya-Putra et al., 2010; Sacharidou et al., 2010; Stratman et al., 2009). The roles of the mammalian homolog of Pl-MmpL7 imply that the sea urchin membrane type MMPs could participate in both biomineralization and in tube formation during sea urchin skeletogenesis. Identifying the substrate of the sea urchin MMP proteins and their subcellular localization during skeletogenesis could illuminate a core mechanism essential for skeletal formation in echinoderms and possibly in other biomineralizing organisms.

Acknowledgements

We thank the advanced imaging center at Janelia research campus for their help with using the LLSM and in animal maintenance. Specifically, we thank Teng-Leong Chew and John Heddleston for the help with the LLSM, Satya Kuhn for help with animals and reagents and Andrew Cohen and Eric Wait for helpful discussions regarding data analysis. This work was supported by the Israel Science Foundation grant numbers 41/14 and 211/20 (S.B.D.), ISEF fellowship (M.M) and Zuckerman fellowship (M.R.W).

Appendix A. Supplementary data

Supplementary data to this article can be found online at https://doi.org/10.1016/j.ydbio.2021.01.013.

References

Adomako-Ankomah, A., Ettensohn, C.A., 2013. Growth factor-mediated mesodermal cell guidance and skeletogenesis during sea urchin gastrulation. Development 140, 4214–4225.
Beniash, E., Addadi, L., Weiner, S., 1999. Cellular control over spicule formation in sea urchin embryos: a structural approach. J. Struct. Biol. 125, 50–62.
Bourd-Boittin, K., Fridman, R., Fanchon, S., Septier, D., Goldberg, M., Menashi, S., 2005. Matrix metalloproteinase inhibition impairs the processing, formation and mineralization of dental tissues during mouse molar development. Exp. Cell Res. 304, 493–505.
Chen, B.C., Legant, W.R., Wang, K., Shao, L., Milkie, D.E., Davidson, M.W., Janetopoulos, C., Wu, X.S., Hammer 3rd, J.A., Liu, Z., English, B.P., Mimori-Kiyosue, Y., Romero, D.P., Ritter, A.T., Lippincott-Schwartz, J., Fritz-Laylin, L., Mullins, R.D., Mitchell, D.M., Bembenek, J.N., Reymann, A.C., Bohme, R., Grill, S.W., Wang, J.T., Seydoux, G., Tulu, U.S., Kiehart, D.P., Betzig, E., 2014. Lattice light-sheet microscopy: imaging molecules to embryos at high spatiotemporal resolution. Science 346, 1257998.
Chenouard, N., Smal, I., de Chaumont, F., Maska, M., Sbalzarini, I.F., Gong, Y., Cardinale, J., Carthel, C., Coraluppi, S., Winter, M., Cohen, A.R., Godinez, W.J., Rohr, K., Kalaidzidis, Y., Liang, L., Duncan, J., Shen, H., Xu, Y., Magnusson, K.E., Jalden, J., Blau, H.M., Paul-Gilloteaux, P., Roudot, P., Kervrann, C., Waharte, F., Tinevez, J.Y., Shorte, S.L., Willemse, J., Celler, K., van Wezel, G.P., Dan, H.W., Tsai, Y.S., Ortiz de Solorzano, C., Olivo-Marin, J.C., Meijering, E., 2014. Objective comparison of particle tracking methods. Nat. Methods 11, 281–289.
Duloquin, L., Lhomond, G., Gache, C., 2007. Localized VEGF signaling from ectoderm to mesenchyme cells controls morphogenesis of the sea urchin embryo skeleton. Development 134, 2293–2302.
Erwin, D.H., 2020. The Origin of Animal Body Plans: a View from Fossil Evidence and the Regulatory Genome, vol. 147. Development.
Ettensohn, C.A., 2013. Encoding anatomy: developmental gene regulatory networks and morphogenesis. Genesis 51, 383–409.
Gibbins, J.R., Tilney, L.G., Porter, K.R., 1969. Microtubules in the formation and development of the primary mesenchyme in Arbacia punctulata. I. The distribution of microtubules. J. Cell Biol. 41, 201–226.
Gildor, T., Ben-Tabou de-Leon, S., 2015. Comparative study of regulatory circuits in two sea urchin species reveals tight control of timing and high conservation of expression dynamics. PLoS Genet. 11, e1005435.
Gildor, T., Cary, G.A., Lalzar, M., Hinman, V.F., Ben-Tabou de-Leon, S., 2019. Developmental transcriptomes of the sea star, Patiria miniata, illuminate how gene expression changes with evolutionary distance. Sci. Rep. 9, 16201.
Hanjaya-Putra, D., Yee, J., Ceci, D., Truitt, R., Yee, D., Gerecht, S., 2010. Vascular endothelial growth factor and substrate mechanics regulate in vitro tubulogenesis of endothelial progenitor cells. J. Cell Mol. Med. 14, 2436–2447.
Holmbeck, K., Bianco, P., Chrysovergis, K., Yamada, S., Birkedal-Hansen, H., 2003. MT1-MMP-dependent, apoptotic remodeling of unmineralized cartilage: a critical process in skeletal growth. J. Cell Biol. 163, 661–671.
Ingersoll, E.P., McDonald, K.L., Wilt, F.H., 2003. Ultrastructural localization of spicule matrix proteins in normal and metalloproteinase inhibitor-treated sea urchin primary mesenchyme cells. J. Exp. Zool. Comp. Exp. Biol. 300, 101–112.
Ingersoll, E.P., Wilt, F.H., 1998. Matrix metalloproteinase inhibitors disrupt spicule formation by primary mesenchyme cells in the sea urchin embryo. Dev. Biol. 196, 95–106.
Kahil, K., Varsano, N., Sorrentino, A., Pereiro, E., Rez, P., Weiner, S., Addadi, L., 2020. Cellular pathways of calcium transport and concentration toward mineral formation in sea urchin larvae. Proc. Natl. Acad. Sci. U. S. A. 117, 30957–30965.
Kawasaki, K., Buchanan, A.V., Weiss, K.M., 2009. Biomineralization in humans: making the hard choices in life. Annu. Rev. Genet. 43, 119–142.
Killian, C.E., Wilt, F.H., 2017. Endocytosis in primary mesenchyme cells during sea urchin larval skeletogenesis. Exp. Cell Res. 359, 205–214.
Kim, Y.S., Joh, T.H., 2012. Matrix metalloproteinases, new insights into the understanding of neurodegenerative disorders. Biomol Ther (Seoul) 20, 133–143.
Lowenstam, H.A., Weiner, S., 1989. On Biomineralization. Oxford University Press, New York.
Mann, K., Poustka, A.J., Mann, M., 2010a. Phosphoproteomes of Strongylocentrotus purpuratus shell and tooth matrix: identification of a major acidic sea urchin tooth phosphoprotein, phosphodontin. Proteome Sci. 8, 6.
Mann, K., Wilt, F.H., Poustka, A.J., 2010b. Proteomic analysis of sea urchin (Strongylocentrotus purpuratus) spicule matrix. Proteome Sci. 8, 33.
Mao, Y., Satchell, P.G., Luan, X., Diekwisch, T.G., 2016. SM50 repeat-polypeptides self-assemble into discrete matrix subunits and promote appositional calcium carbonate crystal growth during sea urchin tooth biomineralization. Ann. Anat. 203, 38–46.
Mass, T., Giuffre, A.J., Sun, C.Y., Stifler, C.A., Frazier, M.J., Neder, M., Tamura, N., Stan, C.V., Marcus, M.A., Gilbert, P., 2017. Amorphous calcium carbonate particles form coral skeletons. Proc. Natl. Acad. Sci. U. S. A. 114, E7670–E7678.
Morgulis, M., Gildor, T., Roopin, M., Sher, N., Malik, A., Lalzar, M., Dines, M., Ben-Tabou de-Leon, S., Khalaily, L., Ben-Tabou de-Leon, S., 2019. Possible cooption of a VEGF-driven tubulogenesis program for biomineralization in echinoderms. Proc. Natl. Acad. Sci. U. S. A. 116, 12353–12362.
Murdock, D.J., Donoghue, P.C., 2011. Evolutionary origins of animal skeletal biomineralization. Cells Tissues Organs 194, 98–102.
Murdock, D.J.E., 2020. The 'biomineralization toolkit' and the origin of animal skeletons. Biol. Rev. Camb. Phil. Soc. 95, 1372–1392.
Oliveri, P., Tu, Q., Davidson, E.H., 2008. Global regulatory logic for specification of an embryonic cell lineage. Proc. Natl. Acad. Sci. U. S. A. 105, 5955–5962.
Page-McCaw, A., Ewald, A.J., Werb, Z., 2007. Matrix metalloproteinases and the regulation of tissue remodelling. Nat. Rev. Mol. Cell Biol. 8, 221–233.
Peled-Kamar, M., Hamilton, P., Wilt, F.H., 2002. Spicule matrix protein LSM34 is essential for biomineralization of the sea urchin spicule. Exp. Cell Res. 272, 56–61.
Potente, M., Gerhardt, H., Carmeliet, P., 2011. Basic and therapeutic aspects of angiogenesis. Cell 146, 873–887.
Raff, R.A., Byrne, M., 2006. The active evolutionary lives of echinoderm larvae. Heredity 97, 244–252.
Rao, A., Seto, J., Berg, J.K., Kreft, S.G., Scheffner, M., Colfen, H., 2013. Roles of larval sea urchin spicule SM50 domains in organic matrix self-assembly and calcium carbonate mineralization. J. Struct. Biol. 183, 205–215.
Reznikov, N., Steele, J.A.M., Fratzl, P., Stevens, M.M., 2016. A materials science vision of extracellular matrix mineralization. Nature Reviews Materials 1, 1–14.
Rundhaug, J.E., 2005. Matrix metalloproteinases and angiogenesis. J. Cell Mol. Med. 9, 267–285.
Sacharidou, A., Koh, W., Stratman, A.N., Mayo, A.M., Fisher, K.E., Davis, G.E., 2010. Endothelial lumen signaling complexes control 3D matrix-specific tubulogenesis through interdependent Cdc42- and MT1-MMP-mediated events. Blood 115, 5259–5269.
Sarashina, I., Endo, K., 2006. Skeletal matrix proteins of invertebrate animals: comparative analysis of their amino acid sequences. Paleontol. Res. 10, 311–336.
Stepicheva, N.A., Song, J.L., 2015. microRNA-31 modulates skeletal patterning in the sea urchin embryo. Development 142, 3769–3780.
Stratman, A.N., Saunders, W.B., Sacharidou, A., Koh, W., Fisher, K.E., Zawieja, D.C., Davis, M.J., Davis, G.E., 2009. Endothelial cell lumen and vascular guidance tunnel formation requires MT1-MMP-dependent proteolysis in 3-dimensional collagen matrices. Blood 114, 237–247.
Sun, Z., Ettensohn, C.A., 2014. Signal-dependent regulation of the sea urchin skeletogenic gene regulatory network. Gene Expr. Patterns 16, 93–103.
Urry, L.A., Hamilton, P.C., Killian, C.E., Wilt, F.H., 2000. Expression of spicule matrix proteins in the sea urchin embryo during normal and experimentally altered spiculogenesis. Dev. Biol. 225, 201–213.
Vidavsky, N., Addadi, S., Mahamid, J., Shimoni, E., Ben-Ezra, D., Shpigel, M., Weiner, S., Addadi, L., 2014. Initial stages of calcium uptake and mineral deposition in sea urchin embryos. Proc. Natl. Acad. Sci. U. S. A. 111, 39–44.
Vidavsky, N., Addadi, S., Schertel, A., Ben-Ezra, D., Shpigel, M., Addadi, L., Weiner, S., 2016. Calcium transport into the cells of the sea urchin larva in relation to spicule formation. Proc. Natl. Acad. Sci. U. S. A. 113, 12637–12642.
Vidavsky, N., Masic, A., Schertel, A., Weiner, S., Addadi, L., 2015. Mineral-bearing vesicle transport in sea urchin embryos. J. Struct. Biol. 192, 358–365.
Vu, T.H., Shipley, J.M., Bergers, G., Berger, J.E., Helms, J.A., Hanahan, D., Shapiro, S.D., Senior, R.M., Werb, Z., 1998. MMP-9/gelatinase B is a key regulator of growth plate angiogenesis and apoptosis of hypertrophic chondrocytes. Cell 93, 411–422.
Wait, E., Winter, M., Cohen, A.R., 2019. Hydra image processor: 5-D GPU image analysis library with MATLAB and python wrappers. Bioinformatics 35, 5393–5395.

Weiner, S., Addadi, I., 2011. Crystallization pathways in biomineralization. Annu. Rev. Mater. Res. 41, 21–40.
Wilt, F., Killian, C.E., Croker, L., Hamilton, P., 2013. SM30 protein function during sea urchin larval spicule formation. J. Struct. Biol. 183, 199–204.
Wilt, F.H., Killian, C.E., Hamilton, P., Croker, L., 2008. The dynamics of secretion during sea urchin embryonic skeleton formation. Exp. Cell Res. 314, 1744–1752.
Winter, M., Mankowski, W., Wait, E., Temple, S., Cohen, A.R., 2016. LEVER: software tools for segmentation, tracking and lineaging of proliferating cells. Bioinformatics 32, 3530–3531.
Winter, R.M., Morgulis, M., Gildor, T., Cohen, R.A., Ben-Tabou de Leon, S., 2020. Calcium-vesicles perform active diffusion in the sea urchin embryo during larval biomineralization. bioRxiv. https://doi.org/10.1101/2020.08.14.244053. Accepted to Plos Comp. Biol.
Yoshizaki, K., Yamada, Y., 2013. Gene evolution and functions of extracellular matrix proteins in teeth. Orthod. Waves 72, 1–10.
Zhou, H., Mak, W., Kalak, R., Street, J., Fong-Yee, C., Zheng, Y., Dunstan, C.R., Seibel, M.J., 2009. Glucocorticoid-dependent Wnt signaling by mature osteoblasts is a key regulator of cranial skeletal development in mice. Development 136, 427–436.